EPR study of $Gd^{3+} - O^{2-}$ centres in Cs_2CdF_4, Rb_2CdF_4 and Rb_2ZnF_4 crystals

1996 J. Phys.: Condens. Matter 8 11299

(http://iopscience.iop.org/0953-8984/8/50/050)

J. Phys.: Condens. Matter **8** (1996) 11299–11308. Printed in the UK

EPR study of Gd^{3+}–O^{2-} centres in Cs_2CdF_4, Rb_2CdF_4 and Rb_2ZnF_4 crystals

M Arakawa†, H Ebisu† and H Takeuchi‡

† Department of Physics, Nagoya Institute of Technology, Nagoya 466, Japan

‡ Department of Information Electronics, School of Engineering, Nagoya University, Nagoya 464-01, Japan

Received 21 May 1996, in final form 28 August 1996

Abstract. EPR measurements have been made on as-grown single crystals of Cs_2CdF_4, Rb_2CdF_4 and Rb_2ZnF_4 doped with Gd^{3+} using an X-band spectrometer. In each crystal a new spectrum having a large fine-structure splitting with orthorhombic symmetry is observed. The new centre is ascribed to a Gd^{3+} ion substituted for the divalent cation with an O^{2-} ion at its ligand site in the *c*-plane. In Rb_2ZnF_4, signals from the uncompensated Gd^{3+} centre are not observed, in contrast with the case for Cs_2CdF_4 and Rb_2CdF_4. Formation of the Gd^{3+}–O^{2-} centre in Rb_2ZnF_4 is discussed using the spin-Hamiltonian separation analysis.

1. Introduction

K_2NiF_4-like layered perovskite crystals with the space group D_{4h}^{17} are interesting because of their close relationship to $KNiF_3$-like cubic perovskite crystals. Figure 1 shows the unit cell of the structure, which may be regarded as a two-dimensional network of NiF_6 octahedra sharing corners, in contrast with the three-dimensional network in cubic perovskite structure. In previous papers [1–7], EPR spectra of the trivalent magnetic impurity ions Gd^{3+}, Cr^{3+} and Fe^{3+} in A_2BF_4 layered perovskite fluorides have been studied systematically by comparing them with those in ABF_3 cubic perovskite fluorides.

In ABF_3 (A = K, Rb, Cs; B = Cd, Ca) crystals, Gd^{3+} ions substitute for host divalent cations having ionic radii close to that of the Gd^{3+} ion. Several kinds of tetragonal and trigonal Gd^{3+} centre are formed in these crystals, where the excess positive charge on the Gd^{3+} ion is locally just compensated by O^{2-} (the Gd^{3+}–O^{2-} centre) [8] at the nearest F^- site, by a Li^+ ion (the Gd^{3+}–Li^+ centre) [9] or by a Na^+ ion (the Gd^{3+}–Na^+ centre) [10] at the nearest B^{2+} site and by a vacancy (the Gd^{3+}–V_A centre) [11] at the nearest A^+ site. In these crystals, tetragonal Gd^{3+} centres with vacancies at the nearest B^{2+} sites (Gd^{3+}–V_B centres) [8, 9, 12] are also formed, though the excess positive charge on Gd^{3+} is locally overcompensated by a B^{2+} vacancy.

For identification of the magnetic impurity centres in low-symmetry crystals, it is important to know the relationship between the fine-structure parameters b_n^m in the spin Hamiltonian and the local environment around magnetic ions. In A_2CdF_4 (A = Rb, Cs) crystals, Gd^{3+} substitutes for Cd^{2+}, similarly to the case for $ACdF_3$ crystals. In these layered perovskite fluorides, EPR spectra of the Gd^{3+}–V_{Cd} and Gd^{3+}–Li^+ centres have been observed with orthorhombic symmetry together with the spectrum of a Gd^{3+} ion without any local compensation in its immediate neighbourhood (uncompensated centres)

0953-8984/96/5011299+10$19.50

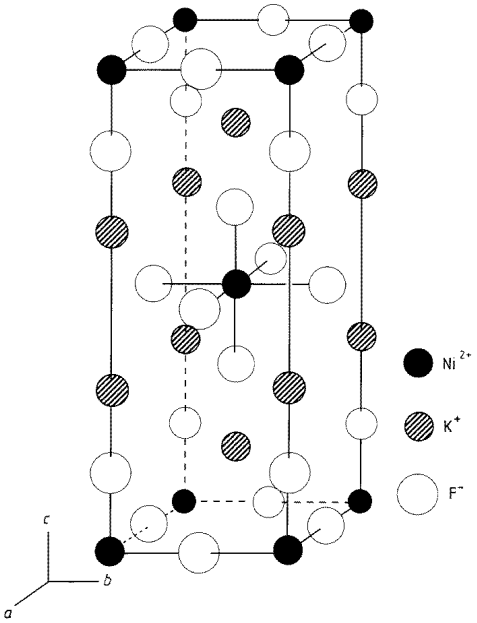

Figure 1. The unit cell of K_2NiF_4-like layered perovskite compounds.

with tetragonal symmetry [4]. For these centres the relationship between the parameters b_n^m and the local environments around Gd^{3+} ions were deduced by separating the fine-structure terms into two uniaxial terms along the *c*-axis and the Gd^{3+}–V_{Cd} (or Li^+) pair direction. Each separated parameter was found to be comparable to the uniaxial parameters for the uncompensated centre observed in the same host crystal or one for the Gd^{3+}–V_{Cd} (or Li^+) centre in $ACdF_3$ crystals [4].

In this paper we will report EPR results for the orthorhombic Gd^{3+} centres newly found in Rb_2CdF_4, Cs_2CdF_4 and Rb_2ZnF_4 single crystals. We will separate the fine-structure parameters of these new centres into two uniaxial parameters and discuss the structures of the centres by comparing the separated uniaxial parameters with those for the Gd^{3+}–V_{Cd} and Gd^{3+}–Li^+ centres [4]. To the authors' knowledge, there have been no EPR reports for Gd^{3+} centres in layered perovskite fluorides with Zn^{2+} host divalent cations. In contrast with those for the Cs_2CdF_4 and Rb_2CdF_4 crystals, the EPR spectra of Rb_2ZnF_4 crystals do not exhibit signals from the uncompensated centre. The formation of the new orthorhombic centre in Rb_2ZnF_4 will be discussed using the results of spin-Hamiltonian separation analysis.

2. Experimental procedures

Single crystals of Cs_2CdF_4, Rb_2CdF_4 and Rb_2ZnF_4 doped with Gd^{3+} were grown in graphite crucibles by the Bridgman technique. Gd metal (99.9%) was added to starting mixtures of BF_2 (B = Cd or Zn) and AF (A = CsF or RbF). The crystals obtained are cleaved easily in the *c*-plane. The measurements were made at room temperature using a JES–FE1XG ESR spectrometer operating in the X-band at the Centre for Instrumental Analysis at Nagoya Institute of Technology. The numerical computations were performed by the computer at the Computation Centre of Nagoya University.

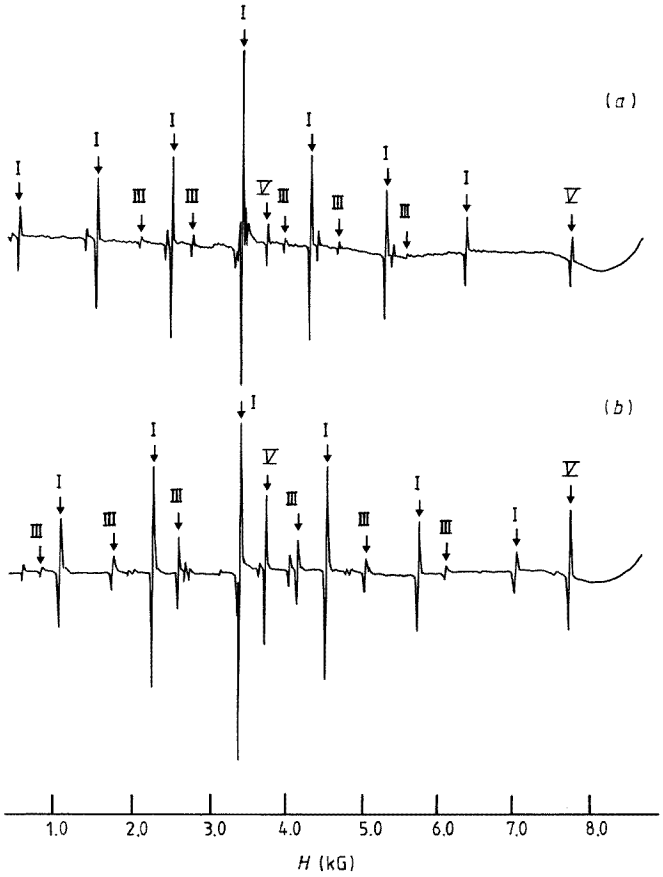

Figure 2. Observed EPR spectra of the Gd^{3+} centres in (*a*) Cs_2CdF_4 and (*b*) Rb_2CdF_4 with $\boldsymbol{H} \parallel [001]$ at room temperature. The arrows labelled V denote the signals from the new orthorhombic centre V together with the centres I and III previously reported [4].

3. Results

For Cs_2CdF_4 and Rb_2CdF_4 doped with Gd^{3+} ions, signals from new magnetic centres with $S = 7/2$ (from now on called centres V) were observed at room temperature, together with those from the uncompensated Gd^{3+} centre (centres I) and the Gd^{3+}–V_{Cd} centre (centres III) [4]. Signals from the centre V disappear in the crystals co-doped with Gd^{3+} and Na^+ used in the previous work [4], where the spectra of the centres I and III were selectively observed. Figure 2 shows the recorder traces of EPR signals at 300 K with the external field parallel to the *c*-axis from as-grown crystals of Cs_2CdF_4 and Rb_2CdF_4. Signals from the centres I, III and V are marked with roman numerals respectively.

The spectra of the centres V in the [100] field direction coincide with those in the [010] direction. When the external field direction is rotated in the *c*-plane, the spectra of the centres V show larger fine-structure splittings than those of the centres III. In figure 3, the high-field signals observed from the centre V in Cs_2CdF_4 are plotted as closed circles against external field directions in the *c*-plane. There are a set of branches marked a and b as shown in figure 3. The branches a and b respectively show maximum total fine-structure

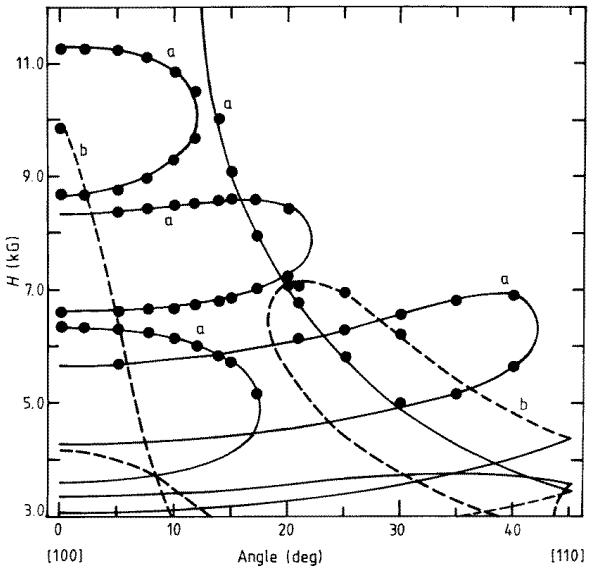

Figure 3. The angular variation of the EPR spectra of the centres V in Cs_2CdF_4 with $\boldsymbol{H}$ in the *c*-plane. The smooth curves indicate the angular variation computed using the parameters for the best fit. The full and dotted lines marked a or b denote a set of calculated branches, where the total fine-structure spreads show maxima in the [100] or [010] field directions respectively.

spread in the field directions parallel to the crystalline [100] and [010] axes. They coincide with each other in the [110] field direction. Another coincidence is also confirmed in the [001] field direction. This indicates the centre V to be of orthorhombic symmetry with charge compensation along a crystalline axis in the *c*-plane.

Figure 4 shows the recorder traces of EPR signals from as-grown crystals of Rb_2ZnF_4 at 300 K. In figure 5 signals from this centre at 300 K are plotted against the external field direction as the closed circles. Two branches a and b are observed, similarly to the case for Cs_2CdF_4 and Rb_2CdF_4. The signals marked a and b in figure 4 respectively correspond to the full and dotted branches in figure 5. Coincidence of these branches for the [001] field direction is also confirmed. From the similarity of the features of the field direction dependence to those for the case of the centres V in Cs_2CdF_4 and Rb_2CdF_4, the signals marked a and b in figure 4 may be ascribed to a Gd^{3+} ion in the same type of centre in the above crystals—that is, centre V. Other weak signals in figure 4 become very weak and eventually disappear in the field directions deviated from the crystalline axes. An isotropic single line (marked x) is seen in figure 4, but the separated fine-structure lines which are expected for the uncompensated centre are not recognized in this field direction. So we conclude that the uncompensated centre is not formed in Rb_2ZnF_4. Unlike in the spectra of Cs_2CdF_4 and Rb_2CdF_4, the signals from the centres I and III disappear within experimental errors.

The spectrum of the centre V can be described by the following spin Hamiltonian with $S = 7/2$:

$$\mathcal{H} = g\beta \boldsymbol{S}\cdot\boldsymbol{H} + \frac{1}{3}(b_2^0 O_2^0 + b_2^2 O_2^2) + \frac{1}{60}(b_4^0 O_4^0 + b_4^2 O_4^2 + b_4^4 O_4^4) + \frac{1}{1260}(b_6^0 O_6^0 + b_6^2 O_6^2 + b_6^4 O_6^4 + b_6^6 O_6^6) \quad (1)$$

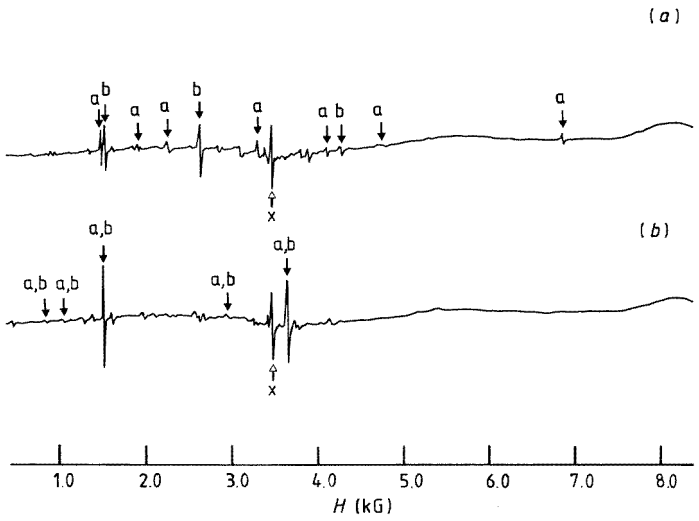

Figure 4. Observed EPR spectra of the Gd^{3+} centres in Rb_2ZnF_4 with (*a*) $\boldsymbol{H} \parallel [100]$ and (*b*) $\boldsymbol{H} \parallel [110]$ at room temperature. a and b each denote a set of signals for the centres V, where the total fine-structure spreads show maxima in the [100] or [010] field directions respectively.

where the O_n^m are the Stevens operators defined by Abragam and Bleaney [13]. The spin Hamiltonian is described in the coordinate system where the z-axis is chosen to be parallel to the direction having maximum total fine-structure spread. The principal x-axis is chosen to be parallel to the c-axis. The branches a and b in figure 3 correspond to the centres V whose z-axes are parallel to the crystalline [100] and [010] axes, respectively. In Cs_2CdF_4 and Rb_2CdF_4, a Cd^{2+} ion is surrounded by the four nearest divalent cations in the c-plane, as shown in figure 1. The direction of the principal z-axis for the centre III is found to be parallel to the crystalline axis in the c-plane [4]. For the centre V in Cs_2CdF_4 and Rb_2CdF_4, the z-axis direction with respect to the crystalline axes is confirmed by simultaneous observation of the centres III. In Rb_2ZnF_4, however, the direction of the principal z-axis relative to the crystalline axes in the c-plane cannot be determined unambiguously from EPR spectra for lack of information on other centres. It was therefore confirmed by x-ray diffraction analysis that the directions of the principal z-axes are parallel to the crystalline [100] or [010] axis.

The spectra observed were fitted to the spin Hamiltonian by the matrix-diagonalization method. The spin-Hamiltonian parameters obtained are listed in table 1. The relative signs among b_n^m-parameters can be uniquely determined. Full and dotted curves in figures 3 and 5 show the theoretical curves calculated using the spin-Hamiltonian parameters listed in table 1. Good agreement of the calculated values of the resonance field with experimental ones is obtained.

4. Discussions

4.1. Spin-Hamiltonian separation analysis

In the previous work on the orthorhombic centres III and IV in Cs_2CdF_4 and Rb_2CdF_4, the surroundings of Gd^{3+} ions were discussed by separating the second-rank fine-structure

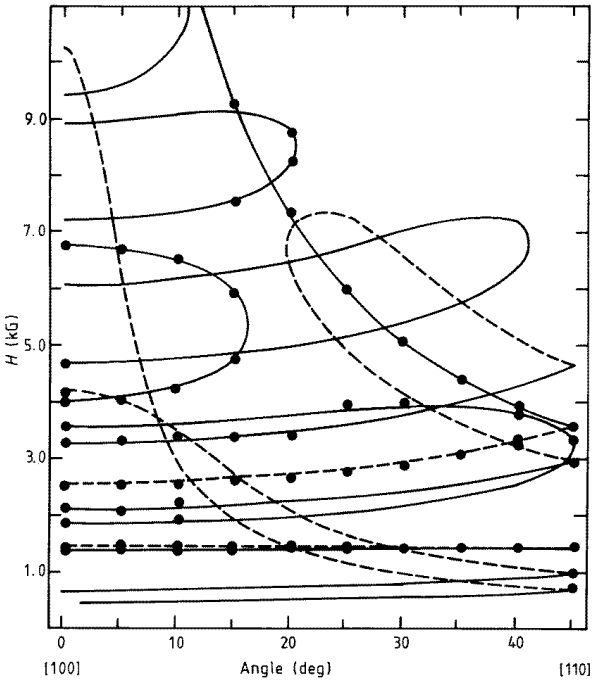

Figure 5. The angular variation of the EPR spectra of the centres V in Rb_2ZnF_4 with $\boldsymbol{H}$ in the *c*-plane. The smooth curves indicate the angular variation computed using the parameters for the best fit. The full and dotted lines show the calculated a and b branches corresponding to the signals marked a and b in figure 4.

Table 1. Spin-Hamiltonian parameters for the orthorhombic Gd^{3+} centres V in Cs_2CdF_4, Rb_2CdF_4 and Rb_2ZnF_4 at 300 K. The upper signs of b_n^m are appropriate as mentioned in section 4.1. The units are 10^{-4} cm^{-1} for b_n^m.

	Cs_2CdF_4	Rb_2CdF_4	Rb_2ZnF_4
g	1.9918(1)	1.9918(1)	1.9918(1)
b_2^0	$\mp$ 2330.6(2)	$\mp$ 2373.1(1)	$\mp$ 2520.5(5)
b_2^2	$\pm$ 808.3(2)	$\pm$ 788.9(2)	$\pm$ 903.2(5)
b_4^0	$\pm$ 1.6(2)	$\pm$ 1.3(1)	$\pm$ 3.8(2)
b_4^2	$\mp$ 2.8(4)	$\mp$ 5.7(5)	$\mp$ 8(1)
b_4^4	$\mp$ 0.5(2)	$\pm$ 3.5(3)	$\mp$ 13(2)
b_6^0	$\mp$ 4.7(2)	$\mp$ 4.8(2)	$\pm$ 0.3(3)
b_6^2	$\pm$ 22(2)	$\pm$ 21(1)	$\mp$ 6(2)
b_6^4	$\mp$ 20.8(9)	$\mp$ 15.2(4)	$\mp$ 18(2)
b_6^6	$\pm$ 36.8(9)	$\pm$ 30.4(9)	$\mp$ 7(6)

terms into two uniaxial terms with the parameters $b_{2a(1)}$ along the *c*-axis and $b_{2a(2)}$ along the Gd^{3+}–V_{Cd} (or Li^+) pair axis in the *c*-plane [4]. Each separated uniaxial parameter was close to the uniaxial parameter for the centre I in the same host crystal and one for the Gd^{3+}–V_{Cd} or the Gd^{3+}–Li^+ centre in the corresponding cubic perovskite crystal. Thus, the spin-Hamiltonian separation analysis is available to identify the magnetic impurity centres in low-symmetry crystals.

Table 2. Values of $b_{2a(1)}$ and $b_{2a(2)}$ derived for the centres V, III, IV, and values of b_2^0 for centre I. The upper signs of $b_{2a(1)}$ and $b_{2a(2)}$ for centres V are appropriate as mentioned in the text. The units are 10^{-4} cm^{-1}.

	Centre V		Centre III		Centre IV		Centre I
	$b_{2a(1)}$	$b_{2a(2)}$	$b_{2a(1)}$	$b_{2a(2)}$	$b_{2a(1)}$	$b_{2a(2)}$	b_2^0
Cs_2CdF_4	± 538.9	∓ 2061.2	-429.1	-227.6	-416.1	-272.3	-443.0
Rb_2CdF_4	± 525.9	∓ 2110.2	-504.2	-207.9	-468.9	-228.1	-549.9
Rb_2ZnF_4	± 602.1	∓ 2219.4	—	—	—	—	—
Reference	This work	This work	[4]	[4]	[4]	[4]	[4]

Table 3. Values of b_2^0 obtained for several kinds of tetragonal Gd^{3+} centre in cubic perovskite fluorides at room temperature. The site column gives the charge-compensation site for the corresponding tetragonal centre. The units for b_2^0 are 10^{-4} cm^{-1}.

Centre	b_2^0	Site	Crystal	Reference
Gd^{3+}–O^{2-}	-2630	F^-	$RbCaF_3$	[8]
Gd^{3+}–V_{Ca}	-314.7	Ca^{2+}	$CsCaF_3$	[9]
	-274.9	Ca^{2+}	$RbCaF_3$	[9]
Gd^{3+}–V_{Cd}	-315.1	Cd^{2+}	$CsCdF_3$	[9]
	-291.3	Cd^{2+}	$RbCdF_3$	[9]
Gd^{3+}–Li^+	-388.3	Ca^{2+}	$CsCaF_3$	[9]
	-318.2	Ca^{2+}	$RbCaF_3$	[9]
	-379.8	Cd^{2+}	$CsCdF_3$	[9]
	-330.2	Cd^{2+}	$RbCdF_3$	[9]

Here, we try to analyse the new orthorhombic centres V in layered perovskite fluorides using the spin-Hamiltonian separation. We separate the second-rank fine-structure terms with orthorhombic symmetry into a uniaxial term with the parameters $b_{2a(1)}$ along the crystalline c-axis (the x-axis) and a uniaxial term with $b_{2a(2)}$ along the z-axis parallel to the direction toward the charge-compensation site in the c-plane. Then, the fine-structure terms written in the xyz coordinate system can be separated as follows:

$$b_2^0 O_2^0(z) + b_2^2 O_2^2(x, y) = b_{2a(1)} O_2^0(x) + b_{2a(2)} O_2^0(z). \tag{2}$$

The term $b_{2a(1)} O_2^0(x)$ denotes the uniaxial term about the x-axis, where $O_2^0(x) = 3S_x^2 - S(S+1)$. Equation (2) is valid when the following conditions are satisfied:

$$b_2^0 = b_{2a(2)} - \frac{1}{2} b_{2a(1)} \qquad b_2^2 = \frac{3}{2} b_{2a(1)}. \tag{3}$$

We can calculate the separated axial parameters $b_{2a(1)}$ and $b_{2a(2)}$ from the observed values of b_2^0 and b_2^2. The results are listed in table 2 together with the separated parameters previously obtained for the centres III and IV and the parameters b_2^0 for the centre I. The separated parameters of $b_{2a(1)}$ are compared with b_2^0 for the corresponding centre I and those of $b_{2a(2)}$ with b_2^0 for the corresponding tetragonal centres in perovskite crystals. The values of b_2^0 obtained previously for several kinds of tetragonal centre in perovskite fluorides are listed in table 3 for comparison. The negative sign of b_2^0 for tetragonal Gd^{3+} centres results from the effective negative charge on the tetragonal axis for compensation of the excess positive charge on Gd^{3+} at divalent cation sites. The separated parameters $b_{2a(2)}$ for the centres III and IV have negative sign, like the b_2^0 for the corresponding tetragonal centre in table 3. For

the centres V, similar negative signs of the separated parameters $b_{2a(2)}$ can be expected. We therefore conclude that upper signs of b_n^m, $b_{2a(1)}$ and $b_{2a(2)}$ in tables 1 and 2 are appropriate for the centres V.

Two things are clear from tables 2 and 3. The first is that the separated parameters $b_{2a(2)}$ for the centre V are an order of magnitude larger than those for the centres III and IV. This indicates that the Gd^{3+} ion may be associated with some sort of charge compensation at one of the ligand sites in the *c*-plane for the centre V in place of a divalent cation site for the centres III and IV. Secondly, the separated parameters $b_{2a(1)}$ for the centre V have the opposite sign to the parameters b_2^0 for the uncompensated centre in the same host crystals. This contrasts with the separated $b_{2a(1)}$-parameters for the centres III and IV, where the parameters are close to the uniaxial parameters for the corresponding centre I as shown in table 2.

The magnitudes of $b_{2a(2)}$ for the centre V are comparable to that of b_2^0 for the Gd^{3+}–O^{2-} centre in $RbCaF_3$ [8]. The formation of the Gd^{3+}–O^{2-} pair is also expected in layered perovskite crystals Cs_2CdF_4 and Rb_2CdF_4 because of the excess charge on the Gd^{3+} ions being just compensated by O^{2-}. The centre V therefore may be ascribed to a Gd^{3+} centre with an O^{2-} ion at one of the ligand sites in the *c*-plane. For the centre V the uniaxial field caused by the excess negative charge of O^{2-} at the ligand site is considered to be dominant. In Cs_2CdF_4 and Rb_2CdF_4, a Cd^{2+} ion is in a fluorine octahedron. The formation of a Gd^{3+}–O^{2-} pair on the *c*-axis is also conceivable—in the same way as those observed in the *c*-plane. But spectra from this pair were not observed. This may be consistent with the fact that the just-compensated Gd^{3+}–V_{Cs} (or Gd^{3+}–V_{Rb}) pair on the *c*-axis was not observed—in contrast to the overcompensated Gd^{3+}–V_{Cd} pair (centres III) observed in these crystals.

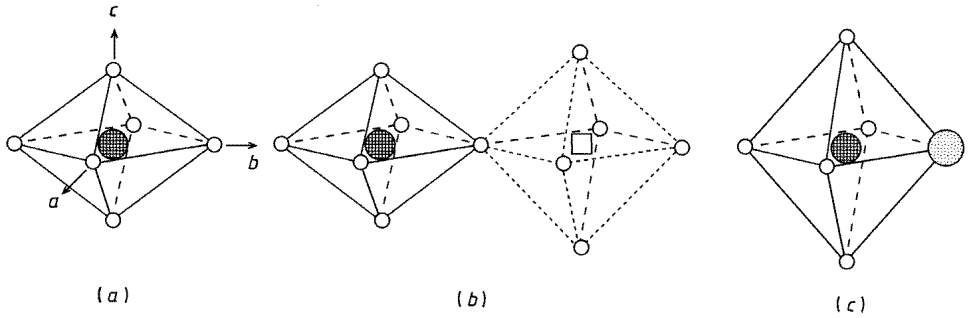

Figure 6. A schematic model of the ligand octahedron for (*a*) the centre I, (*b*) the centre III and (*c*) the centre V.

The negative sign of b_2^0 for the centre I results from the effective negative charge on the *c*-axis. This shows that the ligand octahedron is compressed along the *c*-axis as shown in figure 6(*a*). The negative values of $b_{2a(1)}$ for the centres III and IV indicate that the ligand octahedra may also be compressed (figure 6(*b*)). The positive sign of the separated parameters $b_{2a(1)}$ for the Gd^{3+}–O^{2-} centres suggests that the ligand octahedron is inversely elongated, as shown schematically in figure 6(*c*), by the presence of the O^{2-} ion at the ligand site in the *c*-plane. This indicates that ligand F^- ions along the *c*-axis can move more easily than those in the *c*-plane.

4.2. Formation of the Gd^{3+}–O^{2-} centre in Rb_2ZnF_4

In $KMgF_3$ [14] and $KZnF_3$ [15], Gd^{3+} ions substitute at the K^+ sites in 12-fold coordinations without any local compensation in spite of the large charge misfit. This indicates that Mg^{2+} and Zn^{2+} ions are not replaced by Gd^{3+} due to their small ionic radii. The ionic radius of Rb^+ is large enough to be replaced by Gd^{3+}. First, we consider the possibility that a Gd^{3+}–O^{2-} pair substitutes for a Rb^+–F^- pair in Rb_2ZnF_4. In this crystal a Rb^+ ion is surrounded by nine F^- ions as shown in figure 1. Four Rb–F pairs are in the *c*-plane and the others are not in the plane. If the Gd^{3+}–O^{2-} centre could be formed in place of the Rb–F pair in the *c*-plane, the directions of Gd–O pair axis might be expected to be parallel to the [110] and [1$\bar{1}$0] directions. However, all of the directions of the Gd–O pair axis observed are parallel to the crystalline [100] and [010] axes in the *c*-plane. This is unambiguously confirmed by x-ray diffraction analysis. Thus, the Gd–O pair does not substitute for a Rb–F pair.

Another possibility is substitution for a Zn–F bond although the ionic radius of Zn^{2+} is very small for the substitution of a Gd^{3+} ion. The separated $b_{2a(2)}$-parameters in this crystal are comparable to those for the centre V in Cs_2CdF_4 and Rb_2CdF_4, where Gd–O pairs substitute for Cd–F bonds. The magnitude of $b_{2a(2)}$ for the centre V tends to become larger with decreasing Cd–F distance. This indicates that the Gd–O distance depends on the bond length of the Cd–F pair in the matrix. The fact that the magnitude of the $b_{2a(2)}$ in Rb_2ZnF_4 is larger than that in Rb_2CdF_4 is consistent with this tendency, since the Zn–F bond length (2.0682 Å) [16] is shorter than the Cd–F bond length (2.2009 Å) [16]. We conclude that the orthorhombic centre in Rb_2ZnF_4 is ascribed to a Gd^{3+} ion in sixfold coordination associated with O^{2-} compensation at one of its ligand sites in the *c*-plane, similarly to the case for the centre V in Rb_2CdF_4 and Cs_2CdF_4. It must be emphasized that other centres in sixfold coordinations such as the centres I and III are not observed within experimental errors. This contrasts with the case of those in Cd compounds, where the centre I can be formed more easily than the centre V. The substitution of Gd^{3+} for Zn^{2+} is allowed only by the presence of the O^{2-} ion at the ligand site in the *c*-plane. To the authors' knowledge this centre represents the first EPR report on a Gd^{3+} ion substituted for Zn^{2+} in perovskite-type fluorides.

In layered perovskite fluorides the crystals can be easily cleaved parallel to the *c*-plane. The ligand ions on the *c*-axis may move more easily than those in the *c*-plane. As mentioned in section 4.1, the separated parameters $b_{2a(1)}$ change their sign from negative for the centres III and IV to positive for the centre V in the same layered perovskite crystals. This shows that the ligand F^- ions on the *c*-axis may be deviated away from the Gd^{3+} ion by the presence of the excess negative charge of the O^{2-} ion in the *c*-plane. The deviations enlarge the space at the Zn^{2+} site to be replaced by the Gd^{3+} ion. As a result, the ligand octahedron may be elongated along the *c*-axis as shown in figure 6(*c*). The formation of a Gd^{3+}–O^{2-} centre in Rb_2ZnF_4 is consistent with the positive sign of the separated $b_{2a(1)}$-parameters which shows the elongation of the ligand octahedron.

5. Conclusions

The orthorhombic Gd^{3+} centres newly found in Rb_2CdF_4 and Cs_2CdF_4 crystals have been analysed by the spin-Hamiltonian separation method. The centre has been identified as the Gd^{3+}–O^{2-} pair substituted for a Cd^{2+}–F^- bond in the *c*-plane. The separated parameter $b_{2a(1)}$ has the opposite sign to b_2^0 for the uncompensated centre in each matrix. The ligand octahedron is considered to be elongated along the *c*-axis by the presence of the nearest-

neighbour O^{2-} ion in the *c*-plane. A similar formation of an Gd^{3+}–O^{2-} centre is found in Rb_2ZnF_4 without formation of the uncompensated Gd^{3+} centre. This centre constitutes the first report of Gd^{3+} substituted for Zn^{2+} in sixfold coordination in perovskite fluorides. The substitution of Gd^{3+} for Zn^{2+} is allowed only by the presence of O^{2-} at the ligand site on the crystalline *a*- or *b*-axes. The elongated ligand octahedron makes it possible for a Gd^{3+} ion to substitute for Zn^{2+}, since the space for the Gd^{3+} is enlarged.

Acknowledgments

The authors are very grateful to Dr Masahiro Mori for useful measurements of x-ray diffraction. This work was supported by a Grant-in Aid for Scientific Research on Priority Areas: 'New Development of Rare Earth Complexes', No 07230236, from The Ministry of Education, Science and Culture.

References

[1] Takeuchi H, Arakawa M, Aoki H, Yosida T and Horai K 1982 *J. Phys. Soc. Japan* **51** 3166–72
[2] Takeuchi H and Arakawa M 1983 *J. Phys. Soc. Japan* **52** 279–83
[3] Arakawa M, Ebisu H and Takeuchi H 1986 *J. Phys. Soc. Japan* **55** 2853–8
[4] Takeuchi H, Arakawa M and Ebisu H 1987 *J. Phys. Soc. Japan* **56** 4571–80 (erratum: 1990 **59** 2297)
[5] Arakawa M, Ebisu H and Takeuchi H 1988 *J. Phys. Soc. Japan* **57** 2801–4
[6] Takeuchi H, Ebisu H and Arakawa M 1991 *J. Phys. Soc. Japan* **60** 304–12
[7] Takeuchi H, Arakawa M and Ebisu H 1991 *J. Phys.: Condens. Matter* **3** 4405–20
[8] Buzaré J Y, Fayet-Bonnel M and Fayet J C 1981 *J. Phys. C: Solid State Phys.* **14** 67–81
[9] Arakawa M, Ebisu H and Takeuchi H 1985 *J. Phys. Soc. Japan* **54** 3577–83
[10] Arakawa M, Ebisu H and Takeuchi H 1995 *J. Phys. Soc. Japan* **64** 1356–62
[11] Takeuchi H, Arakawa M and Ebisu H 1995 *J. Phys.: Condens. Matter* **7** 1417–26
[12] Arakawa M, Aoki H, Takeuchi H, Yosida T and Horai K 1982 *J. Phys. Soc. Japan* **51** 2459–63
[13] Abragam A and Bleaney B 1970 *Electron Paramagnetic Resonance of Transition Ions* (Oxford: Clarendon)
[14] Abraham M M, Finch C B, Kolopus J L and Lewis J T 1971 *Phys. Rev.* B **3** 2855–64
[15] Arakawa M, Ebisu H, Yosida T and Horai K 1979 *J. Phys. Soc. Japan* **46** 1483–7
[16] Schrama A H M 1973 *Physica* **68** 279–302